A Bio-Energetic Model for North Atlantic Right Whales: Locomotion, Anatomy and Diving Behavior

Prof. Douglas Nowacek
Duke University Marine Laboratory
135 Duke Marine Lab Road
Beaufort, NC
phone: (252) 504-7588 fax: (252) 504-7648 email: dpn3@duke.edu

Award Number: N000140610576 / N000140811222

LONG-TERM GOALS

1. Measure the physical forces (drag, lift, buoyancy) inherent in right whale locomotion

2. Place these forces in the context of a free-ranging whale by extrapolating them to a seasonal behavioral budget.

3. Understand whether the costs of locomotion could outweigh the energetic intake of right whales.

OBJECTIVES

During this project, we investigated the physical forces that right whales experience in their marine environment and the biological adaptations of these whales to these forces. In comparison to locomotion in a terrestrial environment, energy for marine locomotion is predominately directed towards overcoming the forces of drag and buoyancy (instead of the force of gravity). North Atlantic right whales (*Eubalaena glacialis*) have been characterized as slow-swimming cetaceans that trade off speed for power and therefore may use considerable amounts of energy to swim. We explored (1) the forces generated by swimming right whales during different behaviors, (2) how these forces vary with the morphological variation observed within and between right whale species, and (3) estimating whether changes in the behavioral dive budgets of these animals could increase their energetic requirements for locomotion.

APPROACH

Hydrodynamic forces are typically measured in the controlled environment of a laboratory, but the large size and high mobility of right whales make measurement of flow from an actual animal impossible. Recent work in the field of computational fluid dynamics (CFD) uses Reynolds-averaged Navier-Stokes equations to numerically simulate the flow of a fluid around a representative geometry and provides an estimation of the hydrodynamic forces involved in the motion of fluid around shapes of interest. We used a CFD flow solver to model the drag and lift generated by a swimming right whale. This methodology will also allow us to investigate the flow and its consequent forces through the mouth of a ram-feeding right whale. Key individuals involved in this work are Dr. Mark Sussman, Associate Professor of Mathematics at Florida State University, who is the author of the CLSVOF flow solver and Dr. Gordon Erlebacher, Associate Professor in the Department of Scientific Computing at Florida State University, who has provided visualization software and code to plot the results of the

Report Documentation Page

Form Approved
OMB No. 0704-0188

1. REPORT DATE	2. REPORT TYPE	3. DATES COVERED
2008		**00-00-2008 to 00-00-2008**

4. TITLE AND SUBTITLE	5a. CONTRACT NUMBER
A Bio-Energetic Model for North Atlantic Right Whales: Locomotion, Anatomy and Diving Behavior	5b. GRANT NUMBER
	5c. PROGRAM ELEMENT NUMBER
6. AUTHOR(S)	5d. PROJECT NUMBER
	5e. TASK NUMBER
	5f. WORK UNIT NUMBER
7. PERFORMING ORGANIZATION NAME(S) AND ADDRESS(ES) **Duke University Marine Laboratory,135 Duke Marine Lab Road,Beaufort,NC,28516-9721**	8. PERFORMING ORGANIZATION REPORT NUMBER
9. SPONSORING/MONITORING AGENCY NAME(S) AND ADDRESS(ES)	10. SPONSOR/MONITOR'S ACRONYM(S)
	11. SPONSOR/MONITOR'S REPORT NUMBER(S)

12. DISTRIBUTION/AVAILABILITY STATEMENT
Approved for public release; distribution unlimited

13. SUPPLEMENTARY NOTES

14. ABSTRACT

15. SUBJECT TERMS

16. SECURITY CLASSIFICATION OF:			17. LIMITATION OF ABSTRACT	18. NUMBER OF PAGES	19a. NAME OF RESPONSIBLE PERSON
a. REPORT	b. ABSTRACT	c. THIS PAGE			
unclassified	**unclassified**	**unclassified**	**Same as Report (SAR)**	**13**	

flow simulation. Doctoral student Austen Duffy created code to animate the static whale geometries, and doctoral student Anna McGregor has completed the analysis of diving behavior and the buoyant force measurements. Post-doctoral researcher Ross McGregor performed the morphometric analyses as well as adjusted the whale geometries to accurately represent a North Atlantic right whale.

The results of the CFD flow simulation provided estimates for individual static conditions. In order to place those results in a more realistic context for a large migratory cetacean, we used digital archival tags to obtain high resolution records of the diving behavior of free-ranging North Atlantic right whales. These tags allowed us to monitor the behavior of individual whales over multiple hours and estimate the frequency and duration of those behaviors that are related to locomotion, such as foraging and traveling. The hydrodynamic forces measured from the CFD model will then be applied to the behavioral patterns recorded by the tag and provide an estimate of how much energy an individual right whales requires to swim and feed during the course of a summer foraging season. This behavioral model can then be adjusted to explore how increases in travel time between foraging patches can influence the longer term energetic balance of an individual.

WORK COMPLETED

1. Completed work on quantifying the level of variation in the body shape of right whales

2. Extended dive classification analysis to determine the occurrence of foraging and non-foraging behaviors and, in lieu of better metrics to verify foraging events, determine which behavioral parameters define those stereotypic patterns in movement

3. Static up- and downstroke geometries of whale were interpolated to create a single animated version that simulates the complete fluke stroke for inclusion in the CFD simulation

4. Added particle tracking code to flow solver so that the resolution of flow fields close to the surface of the whale geometry was improved

5. Completed measurements of buoyant force of blubber

6. Paper on inter- and intraspecies morphological variation in Eubalaena species reaching completion

RESULTS

1. **Morphological variation**: Morphometric measurements of all three species of right whale were obtained with aerial photogrammetry, necropsy records and whaling data (Angell, 2006; Best and Rüther, 1992; Moore et al., 2004; Omura et al., 1969; Perryman and Lynn, 2002). Those measurements of body size that influence hydrodynamic performance in the marine environment (body length, body width, fluke span, fluke area and mass) were complied and then used to calculate proportional measurements of fineness ratio and aspect ratio. Our model whale geometry, which was created for use in the CFD solver, was also used to derive measurements of body mass, volume and surface area. The resulting measurements were compared in three ways; (1) between right whale species (*Eubalaena glacialis, E. australis* and *E. japonica*), (2) between individual *E. glacialis* of different ages, and (3) between individual female *E. glacialis* at different reproductive stages.

2. **Additional dive analyses**: Our previous work included a quantitative analysis of the diving behavior of North Atlantic right whales, building on studies that characterized their diving behavior as changes in depth over time (Winn et al., 1995) and attempted to relate stereotyped movements between the surface and depth with observations of whale behavior at the surface (Baumgartner and Mate, 2003). We continued our analysis of right whale dive behavior to determine whether dive shapes can be related to foraging and nonforaging behaviors based on swimming parameters identified by optimal foraging models (Houston and Carbone, 1992; Mori and Boyd, 2004; Simpkins et al., 2001) and not solely on the shape of the time-depth profile as many previous studies on the functional classification of dive shapes have done (Lesage et al., 1999; Martin et al., 1998). This analysis will help determine the frequency and duration of foraging, because, as ram filter-feeders, right whales do not use discrete movement patterns or vocalize when pursuing or capturing their prey, as odontocete cetaceans and pinnipeds do (Aguilar Soto et al., 2008; Miller et al., 2004).

For this analysis, three-dimensional movements of free-ranging right whales were recorded with digital archival tags (Dtags) (Johnson and Tyack, 2003). Individual dives and their constituent dive phases were determined from these records by changes in their time-depth profiles. Dives were classified into three groups according to their shape standardized for maximum depth and duration with a k-means clustering algorithm, which has been shown to be the most robust method of classifying dives into stereotyped patterns in their time-depth profile (Schreer et al., 1998). A series of swimming parameters known to influence diving efficiency were measured from each phase of each dive, including duration, maximum pitch, vertical velocity, stroke rate, path linearity and maximum and minimum depth. Age and sex have been shown to influence the frequency of dive shapes in other species (Baechler et al., 2002), so a linear mixed model was used to determine which swimming parameters differed between those dive shapes while compensating for differences in individual, age and sex. The first type of dive appears to optimize foraging opportunities, the second type appears to be related to nonforaging behaviors and the third to low-quality foraging where animals are searching for new foraging areas. This analysis also allowed us to determine where animals are at highest risk to human activity by quantifying the amount of time spent in different portions of the water column (Figure 1). Animals spending the largest portion of their dives at depth, during U-shaped dives, are more at risk of entanglement in bottom lines than those making repeated V-shaped dives where the potential of entanglement in the vertical fishing lines is much greater.

3. **Animated fluke stroke**: One advantage of the coupled level-set volume of fluid flow solver (CLSVOF) is the inclusion of a time variable in the code, enabling movements of the geometry to be included in the flow solver (Sussman et al., 2007). Our initial simulations consisted of several static geometries placed into a steady-state flow, and these simulations showed differences in the pressure distributions on the surface of the animal and the flow velocity around the animal. However, these static geometries do not account for the flow prior to or following those positions, incorporating an artificial element into the solutions. We created an animated model geometry that incorporates the neutral, tail-up and tail-down positions into one fluid sequence (Video 1). A connective algorithm was used to modify the three static geometries, so that when one point on the surface of the whale geometry was moved, the change in location would be evenly shared between all points connected to it. The magnitude of any changes was exponentially decreased with increasing distance from the one that was moved. In addition to an animated model that contained only fluking motions, we also made a model that contained body oscillations (Videos 2–3). Following the work of Fish (2003), oscillations of the rostrum were in phase with those of the flukes, and much less vertical displacement was added at the rostrum in comparison to that of the flukes. Video analysis of a captive bottlenose dolphin was used to follow the relative positions of the fluke tip and the insertion of the flukes at the peduncle as the

dolphin swam horizontally (Fish, 1998), providing a rough guide for the horizontal position and angle of the flukes relative to the peduncle throughout a fluke stroke (Figure 2). Transverse flexibility was also incorporated into the animation, and the fluke tips moved downwards when the flukes themselves were moving up. Angled wing tips have been shown to decrease induced drag by preventing vortices from being shed by the wing tips (Tucker, 1995), and fluke tip flexibility may serve a similar function for cetaceans. While no accurate measurements were available for the magnitude of the displacement or the amount of the fluke that deflects, tip flexibility was incorporated into the animation.

4. **Particle path tracker**: Our flow simulation is based on a coupled level set/volume-of-fluid method for incompressible flow (Sussman, 2005), and basic features of the flow around the whale are visible from the results of this simulation. In order to identify small scale patterns in flow around the animal, a particle tracker has been added to the code. The particle tracker algorithm simulates the movement of individual particles past the geometry and permits flexibility in the number and position of particles used in the simulation each time. The numerical output of the particle tracker was visualized with Avizo, formerly Amira, software (Mercury Computing, Inc.) (Figure 3). The particle tracker feature greatly increased our ability to follow the flow within detailed areas of the geometry, such as through the baleen in the open-mouthed whale (Figure 4). Initial simulations of particle tracks through the whale's mouth have shown surprising levels of detail (Figures 5–6). Flow entered through the wide opening at the front of the mouth but exited at the top of the arch in the jaw, not from the back of mouth near the eye, as suggested by Werth (2004) (Figures 7–8). The results of our CFD simulations indicated that the Venturi effect may not be the principal force behind the flow through the mouth of a right whale. Therefore, the shape of a right whale mouth may not be anatomically adapted to offset potentially high levels of drag generated by the baleen. The curvature of the baleen racks does seem to influence the flow of water inside the baleen and above the tongue (Lambertsen et al., 2005), as particles that enter the top of the mouth follow the internal curvature inside the mouth (Figures 9–10).

5. **Buoyant force measurements**: Samples of blubber from two stranded North Atlantic right whales were obtained from Woods Hole Oceanographic Institution, and the buoyancy of these samples in seawater was calculated following the protocol of Fish et al. (2002) (Figure 11). Each sample was divided approximately in half, and the buoyancy of those four blubber pieces was calculated with the following formula:

$$F_b = 9.8 \times (m_{air} - m_{water})$$

All samples were measured in seawater at a temperature of 10^{o}C, close to that of summertime water temperatures in the Bay of Fundy. The resulting buoyancy forces were averaged for samples from each animal, and the measurements were found to be 1.62 N and 1.84 N, which averaged to 1.73 N per 500 g sample. These measurements demonstrated that right whale blubber, even in a somewhat degraded state, is considerably positively buoyant, supporting the findings of Nowacek et al. (2001).

6. **Morphometric analysis paper**: Early documentation suggested that clear differences in size were present between geographically separated populations of right whales (Omura et al., 1969). Recent genetic work determined that three genetically distinct populations exist (Rosenbaum et al., 2000), but this work did not explore the potential for morphologic variation between and within these three species. This manuscript complies morphological data on all three species from necropsy reports, aerial photogrammetry measurements and whaling records to determine whether suggested size differences are present between the three species of right whale.

Several more steps are necessary before this project is entirely complete. Our work plan to complete the project consists of the following:

1. Obtain discrete values of drag and lift from the flow solver for all whale geometries.

2. Improve the animated swimming geometry to accurately reproduce the fluking motion.

3. Combine the measurements of hydrodynamic forces from the CFD model with the behavioral budgets of foraging versus nonforaging time recorded with the archival tag

4. Model the influence of changes in ratio of foraging time to non-foraging time on the ratio of energy saved to energy used. If prey aggregations are becoming smaller and/or more separated, whales may have to increase their searching or traveling effort between patches at the expense of time spent foraging. Whether such changes in the typical behavioral budget of this species influence its energetic balance can be determined.
Specific areas for improvement within these steps are the following:

1. The adaptive mesh refinement (AMR) function within the flow solver increases the mesh resolution near the surface of the geometry where most of the changes in flow occur. Decreases in mesh size occur further from the surface to reduce processing demands. However, the mesh size of the flow solver is currently too low in resolution for the spaces between the baleen, so the resulting simulation consists of flow directed between the outer lip and the tongue as it passes from the large opening at the front of the mouth to the smaller opening at the back. Flow must be passing through the baleen in order to sieve prey from water, so this addition to the flow solver is necessary.

2. Work must be continued on the animated geometry, as the static geometries that represented maximum and minimum fluke displacement did not include a fluid movement of the flukes. The current animation includes a horizontal fluke insertion to fluke tip alignment, and work on the cambering of bottlenose dolphin flukes has shown considerable chordwise bending occurs during the fluke stroke (Fish et al., 2006). We plan to improve the path of the flukes when the peduncle changes direction of movement by maintaining a delay in the horizontal alignment between the insertion and the tip. Figures 12 and 13 show the relative position of the tip and insertion in the tailstock recorded from a captive bottlenose dolphin. When the insertion is at its maximum point in the fluke stroke, the fluke tip has not yet reached its maximum displacement. As the insertion of the flukes begins to travel downwards, the maximum displacement of the fluke tip occurs, followed by the realignment of these two points throughout the rest of the downstroke. Similar changes will be applied to the upstroke.

RELATED PROJECTS

No projects related have been initiated at this time.

REFERENCES

Aguilar Soto N, Johnson MP, Madsen PT, Diaz F, Domínguez I, Brito A, Tyack P. 2008. Cheetahs of the deep sea: deep foraging sprints in short-finned pilot whales off Tenerife (Canary Islands). J Anim Ecol 77(5):936–947.

Angell CM. 2006. Body fat condition of free-ranging right whales, *Eubalaena glacialis* and *Eubalaena australis*. Boston, MA: Boston University. 259 p.

Baechler J, Beck CA, Bowen WE. 2002. Dive shapes reveal temporal changes in the foraging behaviour of different age and sex classes of harbour seals (Phoca vitulina). Can J Zool 80(9):1569-1577.

Baumgartner MF, Mate BR. 2003. Summertime foraging ecology of North Atlantic right whales. Mar Ecol Prog Ser 264:123–135.

Best PB, Rüther H. 1992. Aerial photogrammetry of southern right whales, Eubalaena australis. J Zool 228:595-614.

Fish FE. 1998. Comparative kinematics and hydrodynamics of odontocete cetaceans: Morphological and ecological correlates with swimming performance. J Exp Biol 201(20):2867–2877.

Fish FE, Nusbaum MK, Beneski JT, Ketten D. 2006. Passive cambering and flexible propulsors: cetacean flukes. Bioinspiration & Biomimetics 1:S42-S48.

Fish FE, Peacock JE, Rohr JJ. 2003. Stabilization mechanism in swimming odontocete cetaceans by phased movements. Mar Mamm Sci 19(3):515-528.

Fish FE, Smelstoys J, Baudinette RV, Reynolds PS. 2002. Fur does not fly, it floats: buoyancy of pelage in semi-aquatic mammals. Aquat Mamm 28(2):103–112.

Houston AI, Carbone C. 1992. The optimal allocation of time during the dive cycle. Behav Ecol 3:255-265.

Johnson MP, Tyack PL. 2003. A digital acoustic recording tag for measuring the response of wild marine mammals to sound. IEEE J Ocean Eng 28(1):3–12.

Lambertsen RH, Rasmussen KJ, Lancaster WC, Hintz RJ. 2005. Functional morphology of the mouth of the bowhead whale and its implications for conservation. J Mammal 86(2):342-352.

Lesage V, Hammill MO, Kovacs KM. 1999. Functional classification of harbor seal (*Phoca vitulina*) dives using depth profiles, swimming velocity, and an index of foraging success. Can J Zool 77(1):74–87.

Martin AR, Smith TG, Cox OP. 1998. Dive form and function in belugas Delphinapterus leucas of the eastern Canadian High Arctic. Polar Biol 20(3):218–228.

Miller PJO, Johnson MP, Tyack PL. 2004. Sperm whale behaviour indicates the use of echolocation click buzzes 'creaks' in prey capture. Proc Roy Soc B 271:2239–2247.

Moore MJ, Knowlton AR, Kraus SD, McLellan WA, Bonde RK. 2004. Morphometry, gross morphology and available histopathology in North Atlantic right whale (*Eubalaena glacialis*) mortalities (1970–2002). J Cetacean Res Manage 6(3):199–214.

Mori Y, Boyd IL. 2004. The behavioral basis for nonlinear functional responses and optimal foraging in Antarctic fur seals. Ecology 85(2):398-410.

Nowacek DP, Johnson MP, Tyack PL, Shorter KA, McLellan WA, Pabst DA. 2001. Buoyant balaenids: the ups and downs of buoyancy in right whales. Proc R Soc Lond B 268:1811–1816.

Omura H, Ohsumi S, Nemoto T, Nasu K, Kasuya T. 1969. Black right whales in the North Pacific. Scientific Reports of the Whales Research Institute 21:1-78.

Perryman WL, Lynn MS. 2002. Evaluation of nutritive condition and reproductive status of migrating gray whales (*Eschrichtius robustus*) based on analysis of photogrammetric data. J Cetacean Res Manage 4(2):155–164.

Rosenbaum HC, Brownell RL, Brown MW, Schaeff C, Portway V, White BN, Malik S, Pastene LA, Patenaude NJ, Baker CS, Goto M, Best PB, Clapham PJ, Hamilton P, Moore M, Payne R, Rowntree V, Tynan CT, Bannister JL, DeSalle R. 2000. World-wide genetic differentiation of Eubalaena: questioning the number of right whale species. Molecular Ecology 9(11):1793-1802.

Schreer JF, O'Hara Hines RJ, Kovacs KM. 1998. Classification of dive profiles: a comparison of statistical clustering techniques and unsupervised artificial neural networks. Journal of Agricultural, Biological and Environmental Statistics 3(4):383–404.

Simpkins MA, Kelly BP, Wartzok D. 2001. Three-dimensional movements within individual dives by ringed seals (*Phoca hispida*). Can J Zool 79:1455–1464.

Sussman M. 2005. A parallelized, adaptive algorithm for multiphase flows in general geometries. Computers and Structures 83:435-444.

Sussman M, Smith KM, Hussaini MY, Ohta M, Zhi-Wei R. 2007. A sharp interface method for incompressible two-phase flows. Journal of Computational Physics 221:469-505.

Tucker VA. 1995. Drag reduction by wing tip slots in a gliding Harris Hawk *Parabuteo unicinctus*. J Exp Biol 198(3):775-781.

Werth AJ. 2004. Models of hydrodynamic flow in the bowhead whale filter feeding apparatus. J Exp Biol 207:3569–3580.

Winn HE, Goodyear JD, Kenney RD, Petricig RO. 1995. Dive patterns of tagged right whales in the Great South Channel. Cont Shelf Res 15(4/5):593–611.

PUBLICATIONS

In prep McGregor, R., McGregor, A.E., Moore, M., McLellan, W.A., Nowacek, D.P. Body shape variability between and within right whale species (*Eubalaena* sp.) and its influence on hydrodynamic performance.

In prep McGregor, A., Nowacek, D.P., Angell, C.M., Moore, M.J. The influence of blubber thickness on diving behavior of North Atlantic right whales (*Eubalaena glacialis*).

PRESENTATIONS

Nowacek, D.P., McGregor, R., McGregor, A.E., Moore, M., McLellan, W.A.,
Morphological variation in the three *Eubalaena* species: *E. glacialis*, *E. australis* and *E. japonica*: size differs but proportions are constrained by hydrodynamic performance.
North Atlantic Right Whale Consortium Meeting. November 5-7 2008. New Bedford Whaling Museum.

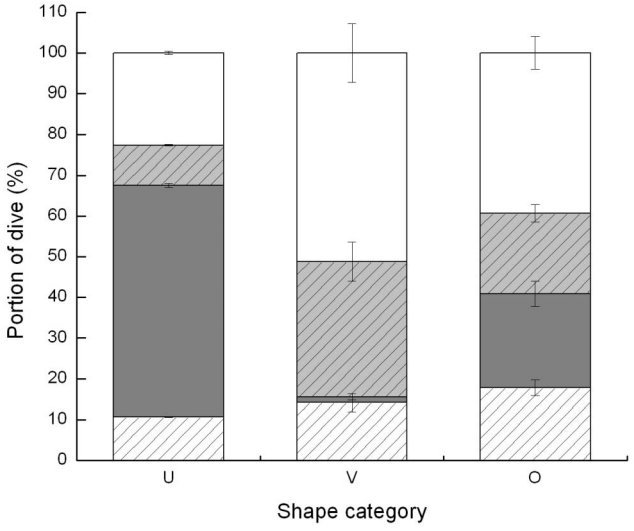

Figure 1. Differences in the portion of each dive spent in each of the following dive phases for three types of right whale dive: descent (hatched white), bottom (solid dark grey), ascent (hatched light grey) and surface (solid white).

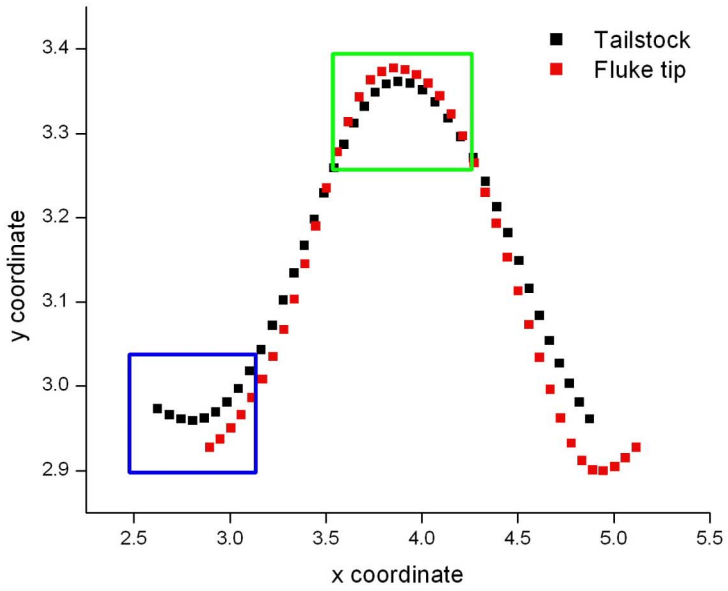

Figure 2. Relative position of the fluke tips (red) and insertion of flukes in tailstock (fluke) over one complete fluke stroke of a captive bottlenose dolphin traveling from right to left (Fish et al., 2003). Blue and green boxes show regions selected for close-up plots in Figures 3 and 4, respectively.

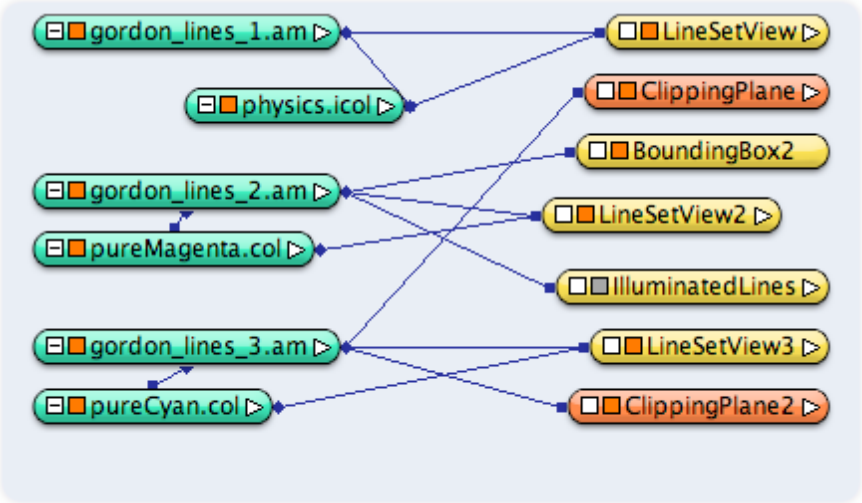

Figure 3. Example of a network script from Avizo that controls the manipulation and visualization of output from flow solver. The green boxes include parameter data, the red and yellow boxes contain action variables, and the blue connecting lines show the relationship between actions and parameters.

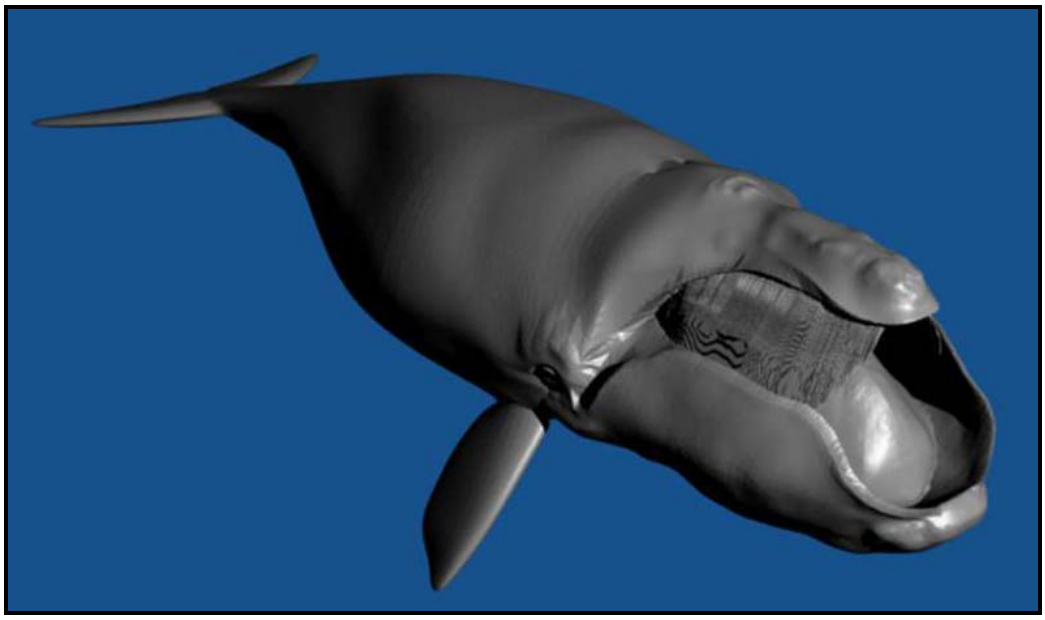

Figure 4. External geometry of open-mouthed whale. Measurements were made of right whales during necropsies, aerial photogrammetry studies and whaling, and applied to the right whale model with Blender software.

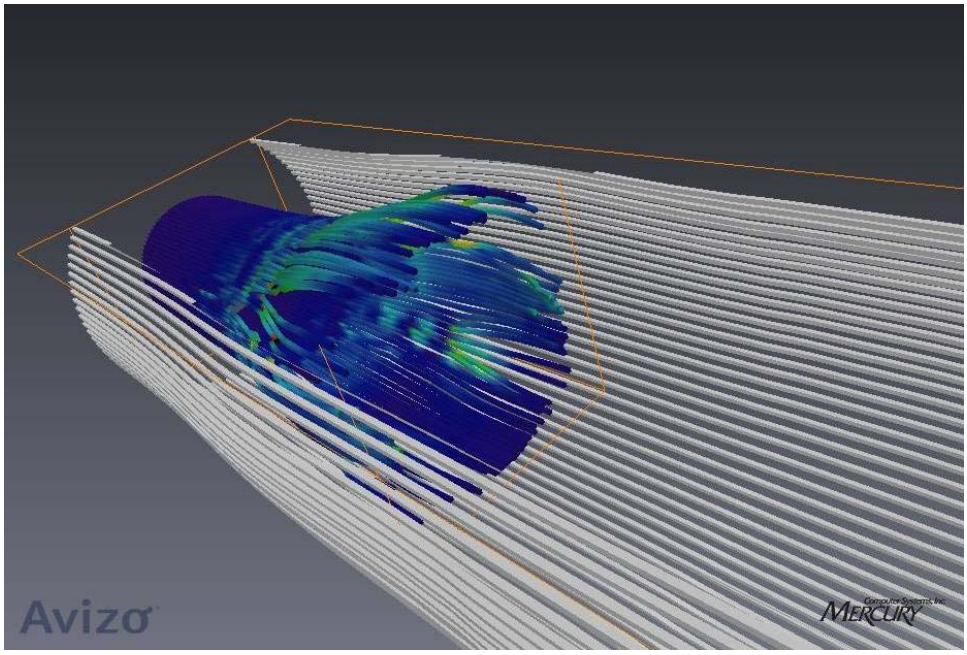

Figure 5. Initial image of pathlines around the head region of neutral whale geometry. Each line represents the path of a virtual particle as it moves with the flow around the geometry. Blue-green color scale represents velocity along the path of particle, and path lines that begin as blue are those representing the fine-scale mesh for near field flow. White path lines represent far field flow, which used a lower resolution mesh. Animal's rostrum is on the left side of the image, and its ventral side is facing up.

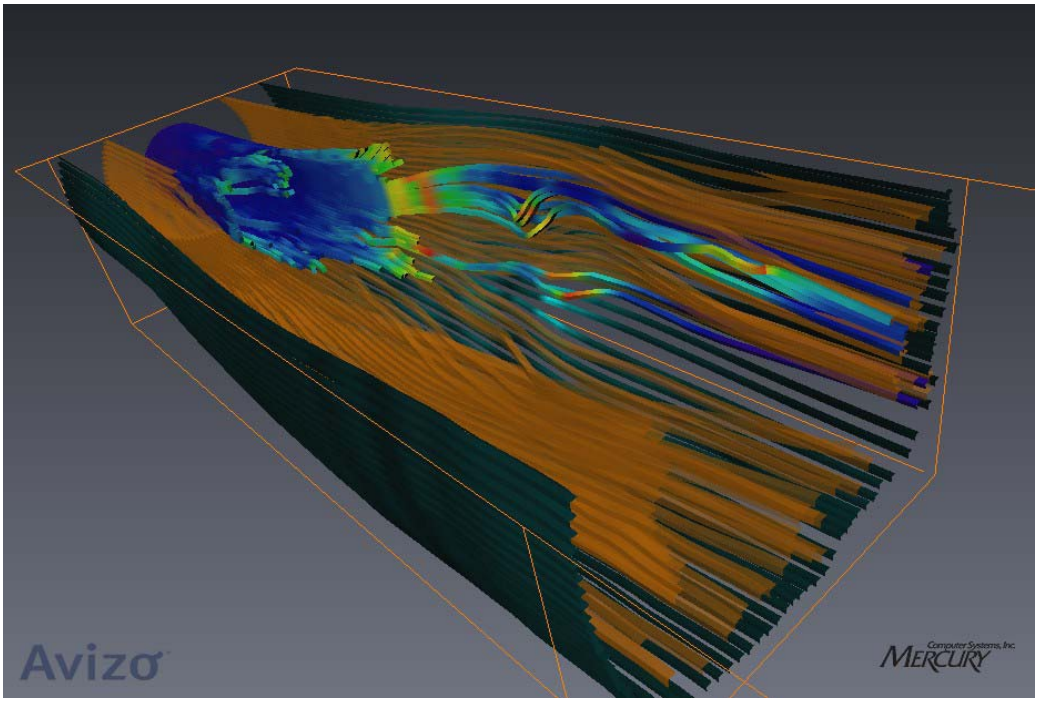

Figure 6. Extension of path lines further along animal's body. Animal is in the same orientation as in Fig. 2. Brown and black path lines represent sequentially lower resolution meshes.

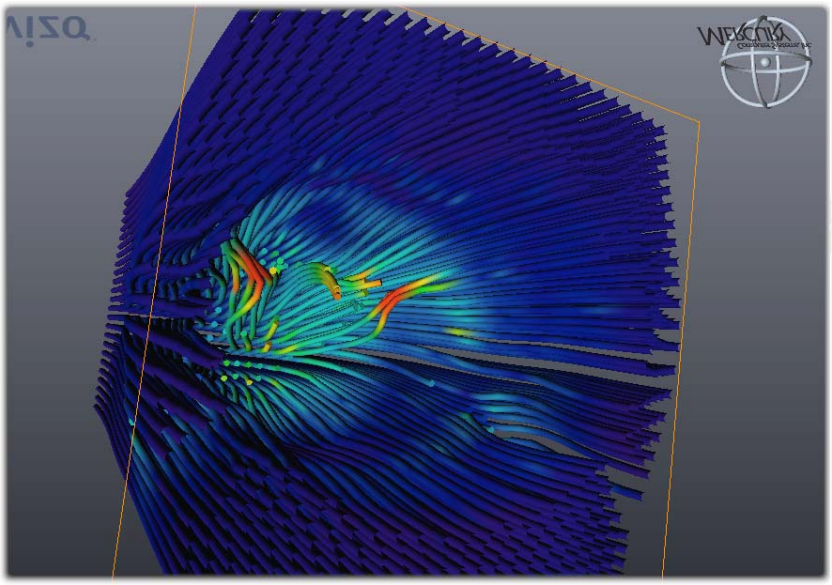

Figure 7. Results from simulation of flow around the head of the open-mouthed whale using a low resolution mesh and particle tracker. External whale geometry has been removed to allow full view of flow. Flow originates at left side of image, and whale is facing to the left. Dark blue shows free stream flow velocity, and colors represent increased flow velocity.

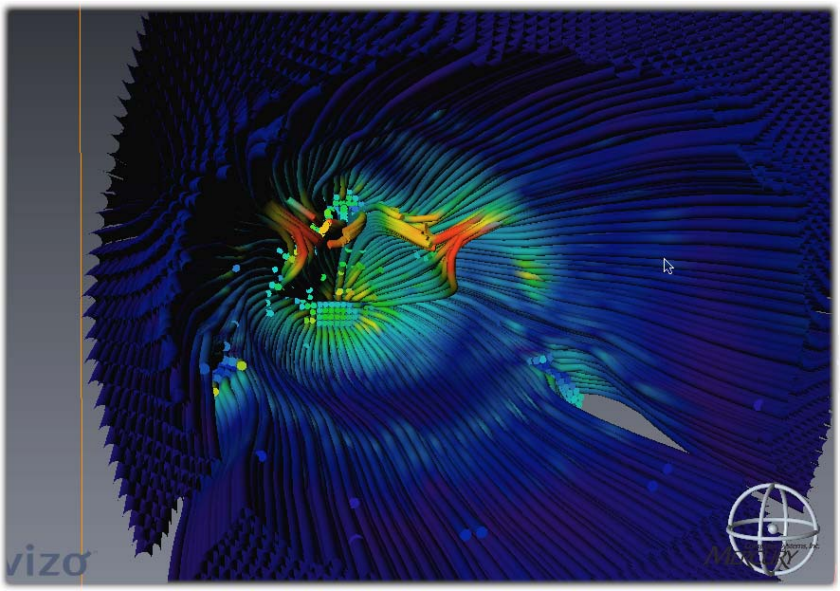

Figure 8. Similar image to Figure 7 with higher resolution particle tracker. Whale geometry is oriented dorsal side up and head pointing away. Large gaps in the flow that appear in the lower left and right corners of the figure show flow splitting around the pectoral fins. Color scale represents velocity along the particle paths, blue corresponding to the lowest velocity and red the highest.

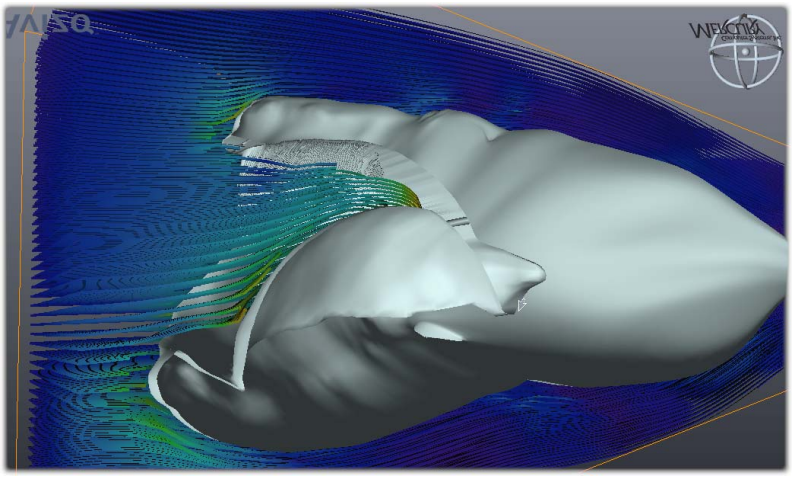

Figure 9. Flow into the open mouth of a right whale, including both particle path lines and the external whale geometry. Image includes only the right half of the animal, and the flow can be seen passing to the far side of the tongue. Flow was originated on the left side of the image. The baleen can be seen as the rough grey surface near the upper left side of the whale geometry, hanging down from the upper jaw. Simulation does not include flow through the baleen, as the resolution of the geometry in that area exceeds the possible mesh resolution of the flow solver.

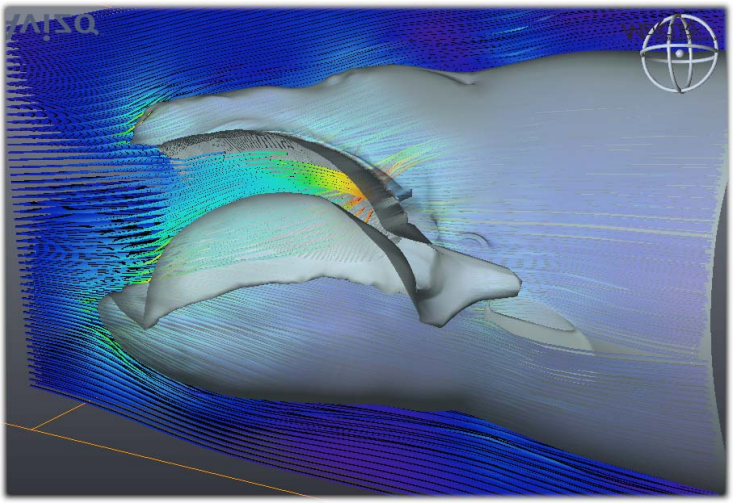

Figure 10. Results from same simulation as Figure 9 viewed from a different perspective. Image shows the animal's right half viewed from inside the whale geometry along the longitudinal midline of the animal. Flow is traveling from the left to the right, and colors represent the velocity magnitude along the particle path.

Figure 11. Experimental setup used to measure the buoyancy of right whale blubber. Blubber sample was cut to a mass in air of approximately 500g, weighed in air and then weighed in in seawater at 10^{o}C. Metal washers were used to submerge the blubber sample completely during the water measurement.